

Lawrence Berkeley National Laboratory

LBL Publications

Title

Optical phase control of coherent pulse stacking via modulated impulse response

Permalink

<https://escholarship.org/uc/item/2df8m25p>

Journal

Journal of the Optical Society of America B, 35(9)

ISSN

0740-3224

Authors

Yang, Yawei
Doolittle, Lawrence
Galvanauskas, Almantas
et al.

Publication Date

2018-09-01

DOI

10.1364/josab.35.002081

Peer reviewed



Optical phase control of coherent pulse stacking via modulated impulse response

Yawei Yang,^{1,*} Lawrence Doolittle,¹ Almantas Galvanauskas,² Qiang Du,¹ Gang Huang,¹ John Ruppe,² Tong Zhou,¹ Russell Wilcox,¹ and Wim Leemans¹

¹Lawrence Berkeley National Laboratory, Berkeley, California 94704, USA

²Center for Ultrafast Optical Science, University of Michigan, Ann Arbor, Michigan 48109, USA

*Corresponding author: yyw721@gmail.com

Received 24 May 2018; revised 22 June 2018; accepted 2 July 2018; posted 3 July 2018 (Doc. ID 331880); published 7 August 2018

To stabilize the combined pulse energy for coherent temporal pulse stacking using interferometer cavities, we have developed a direct cavity phase measurement method based on analysis of the response to modulated probe pulses. An experiment has demonstrated optical phase control within 50 mrad for four cavities, resulting in a combination of 25 pulses with 1.5% root mean square stability over 30 h. © 2018 Optical Society of America

OCIS codes: (140.3298) Laser beam combining; (140.3510) Lasers, fiber; (140.3538) Lasers, pulsed.

<https://doi.org/10.1364/JOSAB.35.002081>

1. INTRODUCTION

Fiber lasers have demonstrated advantages in many applications due to their superior efficiency, stability, and beam quality. However, in high-peak-power applications, nonlinear effects and optical damage limit the extractable energy [1]. Spatial and temporal pulse combination [2] can overcome these limitations, potentially leading to joule-level ultrafast pulses currently only available from bulk amplifiers with low repetition rates. Fiber amplifiers could operate at higher average power, providing kilohertz (kHz) repetition rates and >20% wall plug efficiency, leading to a practical driver for future plasma wake-field accelerators [3,4].

The chirped-pulse amplification (CPA) architecture has enabled large-core-area fiber lasers to produce ultrafast pulses with 0.1–1 mJ energy by stretching the short pulse to ~1 ns to reduce peak power [5,6]. This is still only a fraction of the stored energy that could be extracted if the pulses were tens or hundreds of nanoseconds long [7].

Temporal coherent combination further extends the pulse duration by assembling many pulses in a train passed through the amplifier into one output pulse, which can then be compressed. The divided-pulse amplification technique splits an initial pulse into a train of pulses, then combines them after the amplifier using beam splitters and free-space delay lines [8]. While this has been demonstrated to work [9], the optical complexity of the scheme makes it difficult to combine ~100 pulses, which would be required for full energy extraction.

To reduce the optical complexity, a novel concept has been proposed that coherently combines pulses from a train in an optical cavity and then extracts the energy with a mechanical switch [10]. While the scheme is optically simple, the switch is

a significant challenge. Another concept uses passive Gires-Tournois interferometers (GTI) to combine pulses from a specially phase-coded train [11,12], not requiring a switch. Large numbers of pulses can be added by actively controlling the pulse train phases and the interferometer cavity phases [13,14]. Recently, a train of 81 pulses has been used to extract ~10 mJ from a large-core fiber amplifier [15].

The pulse energy output from this GTI-based coherent pulse stacking (CPS) scheme is sensitive to perturbations of the applied phase modulation, oscillator amplitude, amplifier gain, and alignment stability, among others. One of the main parameters affecting stacking efficiency and thus output energy is the cavity round-trip phase [7], which we address here.

In this paper, we introduce a direct cavity phase detection and control method applicable to the GTI-based CPS scheme, which we call modulated impulse response (MIR). In Section 2 we describe the CPS concept, showing how ~100 pulses can be added using a few optical cavities. Numerical simulation shows the effect of cavity phase errors on the output pulse, motivating the development of an active phase locking method. In Section 3 we introduce the MIR principle and how it is applied in an active locking scheme. In Section 4, we demonstrate the MIR method in a CPS experiment, in which 25 equal-amplitude pulses are stacked into one, using four cavities, for an energy enhancement of 18.4.

2. COHERENT PULSE STACKING AND OPTICAL ROUND-TRIP PHASE

A. Pulse Stacking Concept Overview

The GTI-based CPS scheme stacks a series of phase-modulated pulses into one, using a series of concatenated cavities. Each

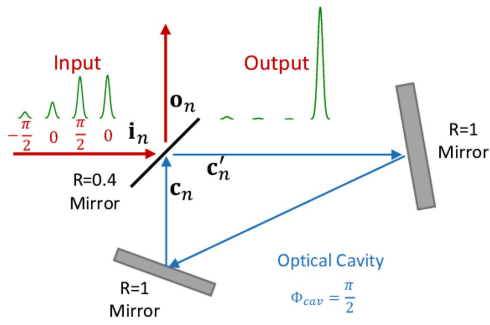


Fig. 1. GTI optical cavity used for coherent pulse stacking. Four pulses with appropriate phase modulation are stacked into one pulse when $\Phi_{\text{cav}} = \frac{\pi}{2}$.

cavity is comprised of one low-reflectivity input–output mirror and other high-reflectivity mirrors to form a cavity with a round-trip delay equal to the pulse interval (or a multiple thereof), as shown in Fig. 1. Characterizing each pulse by the complex electric field amplitude, we write the input pulse as \mathbf{i}_n and the output pulse as \mathbf{o}_n . At the low-reflective mirror, the input pulse \mathbf{i}_n and the pulse in the optical cavity \mathbf{c}_n interfere to form two pulses \mathbf{o}_n and \mathbf{c}'_n , which go to the output and back into the cavity, respectively.

Assuming the interference is lossless, the two pulses \mathbf{o}_n and \mathbf{c}'_n are related to the cavity pulse \mathbf{c}_n and input pulse \mathbf{i}_n according to

$$\begin{pmatrix} \mathbf{o}_n \\ \mathbf{c}'_n \end{pmatrix} = \begin{pmatrix} r & it \\ it & r \end{pmatrix} \begin{pmatrix} \mathbf{i}_n \\ \mathbf{c}_n \end{pmatrix}, \quad (1)$$

where r and t are the mirror field reflection and transmission coefficients ($r^2 + t^2 = 1$), and the reflectivity $R = r^2$. Here, the resonator operates as a delay line. A pulse in the cavity after one round-trip can be written as

$$\mathbf{c}_n = \alpha e^{j\Phi_{\text{cav}}} \cdot \mathbf{c}'_{n-1}, \quad (2)$$

where α is the amplitude loss per round-trip and Φ_{cav} is the optical round-trip phase. The optical round-trip phase determines whether the interference is constructive or destructive. Figure 1 gives an example showing that when $\Phi_{\text{cav}} = \frac{\pi}{2}$, an amplitude- and phase-modulated burst of four pulses can be stacked into one high-intensity pulse.

By combining Eqs. (1) and (2), the output pulse electric field \mathbf{o}_n can be expressed as a difference function of \mathbf{i}_n ,

$$\mathbf{o}_n - r\alpha e^{j\Phi_{\text{cav}}} \cdot \mathbf{o}_{n-1} = r\mathbf{i}_n - \alpha e^{j\Phi_{\text{cav}}} \cdot \mathbf{i}_{n-1}. \quad (3)$$

Using concepts from digital signal processing [16], we modeled the optical cavity. Since stacking occurs on the nanosecond scale, r and Φ_{cav} can be taken as constant during the process. Another assumption is that initially there is no energy stored in the cavity. Under these conditions, the interferometer can be modeled as a linear, time-invariant (LTI) filter, defined by Eq. (3).

In this paper we consider equal-amplitude pulse bursts as input pulses, which minimize peak power (the analysis is also valid for unequal-amplitude trains, which may be needed for maximum energy extraction in a saturating amplifier). We define the energy enhancement factor as the output pulse

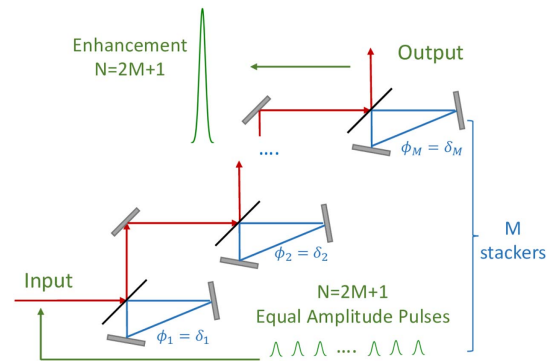


Fig. 2. Sequence of M cascaded pulse stackers combining $N = 2M + 1$ pulses into one high-intensity pulse.

intensity divided by the intensity in each pulse in the train, $\kappa = O_0/I_0$. While the energy enhancement for a single cavity is about 2.5, higher enhancement can be achieved using sequences of optical cavities [11], as shown in Fig. 2.

Given a number M of concatenated cavities of equal length, the number of pulses N that can be stacked into one using these cavities is

$$N = 2M + 1. \quad (4)$$

In addition, the relative phases of the pulses in the train and the round-trip phases of the cavities need to be specified and controlled [7,11].

Table 1 lists a number of optimized equal-amplitude stacking sets with different numbers of cavities.

To extract all the energy in a fiber amplifier while maintaining low nonlinearity, about 100 pulses (each stretched to 1 ns) will be needed. If the stacker were comprised of only one size of cavity, Eq. (4) predicts that 50 cavities would be needed, which is not practical.

Instead, we can cascade several sizes of sequences of cavities, thereby multiplying the enhancement factor [7,11,12]. Figure 3 shows a cascaded, two-stage stacking scheme, with two short cavities in stage one and two longer cavities in stage two, in which 25 equal-amplitude pulses can be stacked into one pulse. In the first stage, the cavity length is one pulse period, and groups of five pulses are stacked, producing five pulses from the 25, separated by five pulse periods. In stage two, the cavities are five times longer, stacking the five pulses from stage one into one final output pulse. We call this a 2 + 2 stacker to identify the cavity arrangement. There are various stacking schemes to combine about 100 pulses into one; three

Table 1. Energy Enhancement with an Increasing Number of Optical Cavities^a

M	N	Enhancement (κ)	Reflectivity (R)
1	3	2.61	[0.39]
2	5	4.66	[0.42, 0.51]
3	7	6.62	[0.48, 0.55, 0.63]
4	9	8.72	[0.52, 0.54, 0.62, 0.68]
5	11	10.7	[0.53, 0.54, 0.57, 0.64, 0.72]

^aThe optimized mirror reflectivity values R are also listed.

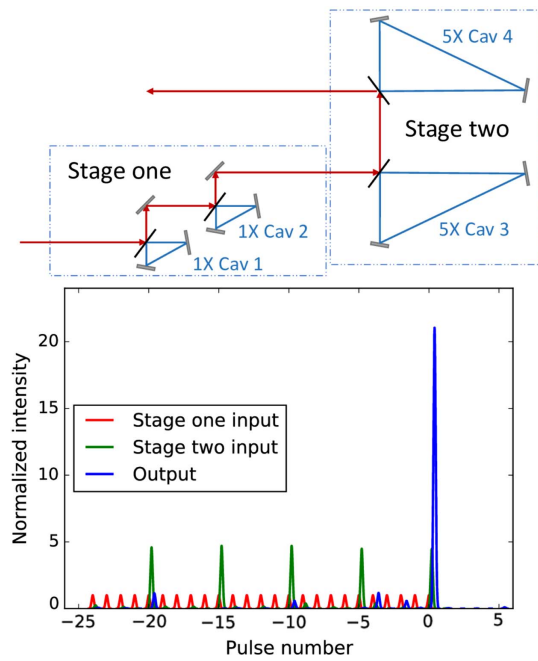


Fig. 3. Multiplexed 2 + 2 stacking schemes. The optical cavity in stage two is 5× as long as in stage one; 25 pulses can be approximately stacked into one pulse with enhancement over 20.

Table 2. Comparison of Three Kinds of Optimized Cascaded Multi-Stage Stacking Schemes

Cavity Set	Cavity Length	Pulse Number	Enhancement
4 + 4	[1×, 9×]	81	77.4 (18.9 dB)
2 + 2 + 2	[1×, 5×, 25×]	125	100.2 (20.0 dB)
4 + 2 + 1	[1×, 9×, 45×]	135	108.1 (20.2 dB)

examples are listed in Table 2. The two-stage, 4 + 4 scheme has been investigated at the University of Michigan [7,13], while at Lawrence Berkeley National Laboratory (LBNL) we explored a three-stage, 2 + 2 + 2 scheme. While efficiency and pre-pulse suppression are worse with the latter scheme, it uses fewer cavities to achieve a higher enhancement.

We can compare cascaded multi-stage CPS schemes with the divided-pulse amplification (DPA) scheme [9,17,18], for a combination of about 100 pulses. In DPA, the number of delay lines k needed to stack, for instance, 128 pulses would be $\log_2 128 = 7$. The longest delay line would be $2^{k-1} = 64$ times the pulse period. By contrast, cascaded CPS can stack 125 pulses using six cavities, the longest of which is 25 pulse periods, or stack 81 pulses with eight cavities no longer than nine pulse periods. With smaller cavities, cascaded CPS has a smaller footprint.

B. Pulse Stacking Stability versus Cavity Phase Error

Random variations of the cavity phases due to thermal or mechanical perturbations will strongly impact the stacking performance. As shown in Fig. 4, phase offset (error) of one cavity in a cascaded-cavity stacking set will decrease the enhancement factor, and the effect is worse for larger numbers of cavities as

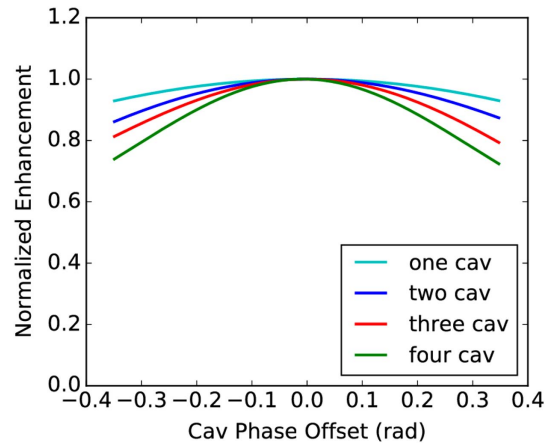


Fig. 4. Normalized enhancement versus single-cavity phase offset. Stacking sets with different numbers of cavities are compared. Only one optical cavity is offset from the exact value in this simulation.

the phase bandwidth narrows. A 0.3 radian phase error in an optical cavity will drop the enhancement by about 20% in a four-cavity stacking set, while the drop will be only 5% for a single-cavity stacker. Thus, all the cavities need to be well controlled in phase, with the requirements becoming more stringent when using multi-cavity cascades.

The cavity phase control accuracy determines the phase noise level during operation, affecting stacked output pulse energy stability, which we describe as an root mean square (RMS) percentage.

We used numerical simulations to analyze the phase dependence of the stacked pulse stability by corrupting the cavity phase values with Gaussian-distributed noise and deriving statistics from 2000 calculations. Both one-stage stacking and cascaded multi-stage stacking were analyzed.

Figure 5(a) shows the energy stability versus cavity phase error per cavity in single-stage stacking sets, which have different numbers of optical cavities with the same optical length. Output pulse energy stability deteriorates at a rate of σ_ϕ^2 with increasing phase error. In addition, this effect worsens as the number of cavities increases, increasing as $M^{1.6}$, where M is the number of cavities. Since the energy enhancement is linear with M , the overall phase sensitivity increases faster than the enhancement. A four-cavity stacking set will have about 1.9 times the enhancement of a two-cavity set, but almost 3 times the stacked pulse instability, given the same phase noise level per cavity. The increasing noise sensitivity as more cavities are added is due to the narrowing phase bandwidth as shown in Fig. 4.

For multi-stage, cascaded stacking arrangements with different length cavities, simulations show that noise sensitivity does not increase significantly when more stages are added. Figure 5(b) shows the stacked pulse energy stability of a two-stage scheme with two cavities per stage, versus cavity phase noise in each stage. Stage one and stage two perform the same function but on different sets of pulses (every pulse versus every fifth pulse). So their phase bandwidths are independent, and the noise sensitivity of one stage does not depend on the other. Both stages need to be controlled but not more precisely than

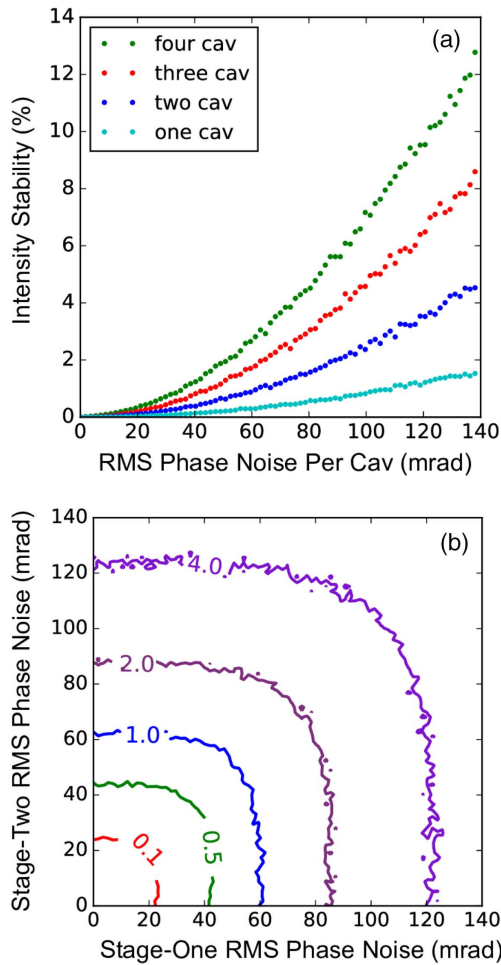


Fig. 5. Calculated stacked pulse energy stability versus cavity phase noise level per cavity in (a) sequence of one-stage stackers and (b) contour plot of stability percentage in a cascaded 2 + 2 pulse stacking scheme. The horizontal and vertical axes are the RMS cavity phase error.

one stage by itself. For example, if the output energy stability must be 1%, the RMS phase noise has to be controlled within 60 mrad in both stages, which is about the same for a single-stage, two-cavity set with 1% output stability, as shown in Fig. 5(a). At our wavelength of 1064 nm, 60 mrad corresponds to 10 nm of cavity length or ~ 2 nm of mirror position drift. Thus, all cavity lengths must be controlled to nanometer (nm)-level accuracy to achieve $\sim 1\%$ stability.

3. MODULATED IMPULSE RESPONSE PHASE DETECTION

A. Phase Control Method Overview

Several cavity phase locking schemes are possible and have been implemented. The initial proof-of-principle coherent pulse stacking demonstration [11] used Pound–Drever–Hall (PDH) locking [19], which results in a simple control method but added optical complexity. A less optically complex scheme is based on the stochastic parallel gradient descent (SPDG) algorithm [20], which uses a single peak power detector to

measure the output pulse energy, while adjusting the cavity phases by the SPDG algorithm to maximize the stacked signal energy [7,21]. However, the SPDG algorithm requires an initial search procedure to find the approximate cavity phase values from which the SPDG algorithm can converge to the maximized stacked energy. Furthermore, since it maximizes the actual stacked signal, the feedback rate cannot exceed the stacking pulse burst repetition rate, which at high energy operation is typically between 1 and 10 kHz.

We have explored a different scheme, which directly measures each cavity's round-trip phase using modulated probe pulses. In this scheme, one detector is added after each cavity, capturing a small portion of light for optical phase detection. For each cavity, a control loop is implemented to lock the cavity phase to any prescribed value, and therefore there is no need for an initial search. This control scheme is scalable to multiple cavities, and modulated probe pulses can be interleaved with the stacking pulse burst in the time domain. Because of this, the feedback rate can be much higher than the stacking pulse burst repetition rate. To derive the cavity phase from probe-burst responses, we have developed a novel cavity phase detection method, which we call “modulated impulse response” or MIR.

B. Modulated Impulse Response Principle

As described in Section A, the pulse stacker can be modeled as a digital filter. Assuming a lossless cavity where $\alpha = 1$, the impulse response, using Eq. (3), can be written as

$$\mathbf{o}_n = r^{n+1} e^{jn\phi} u[n], \quad (5)$$

where $u[n]$ is the unit step. The output pulse phase term $e^{jn\phi}$ is related to the cavity phase, but this cannot be directly measured from the impulse response. In order to transform the phase term into an easily measured amplitude signal, we introduce a probe pulse burst consisting of two equal amplitude pulses,

$$\mathbf{i}_n = \delta[n+1] + \delta[n]e^{j\theta}, \quad (6)$$

where $\delta[n]$ is the unit impulse function, and θ is the phase difference between the two pulses. Using Eq. (3), we can derive the resultant output pulses. The first output pulse is simply a reflection, $\mathbf{o}_{-1} = r$, which will remain constant as Φ_{cav} changes. The second output pulse will be

$$\mathbf{o}_0 = r e^{j\theta} - (1 - r^2) e^{j\phi}, \quad (7)$$

which can be used to observe the cavity phase.

The intensity of the second pulse $O_0 = |\mathbf{o}_0|^2$ is

$$O_0 = (1 - r^2)^2 + r^2 - 2r(1 - r^2) \cos(\phi - \theta), \quad (8)$$

which is a cosine function of the cavity phase. If $\frac{\pi}{2}$ is added to the relative phase between the two pulses in the probe pulse burst,

$$\mathbf{i}_n = \delta[n+1] + \delta[n]e^{j(\theta+\frac{\pi}{2})}, \quad (9)$$

the second output pulse will be

$$\mathbf{o}_0 = \left(r e^{j(\theta+\frac{\pi}{2})} - (1 - r^2) e^{j\phi} \right). \quad (10)$$

The intensity can be written as

$$O_0 = (1 - r^2)^2 + r^2 - 2r(1 - r^2) \sin(\phi - \theta), \quad (11)$$

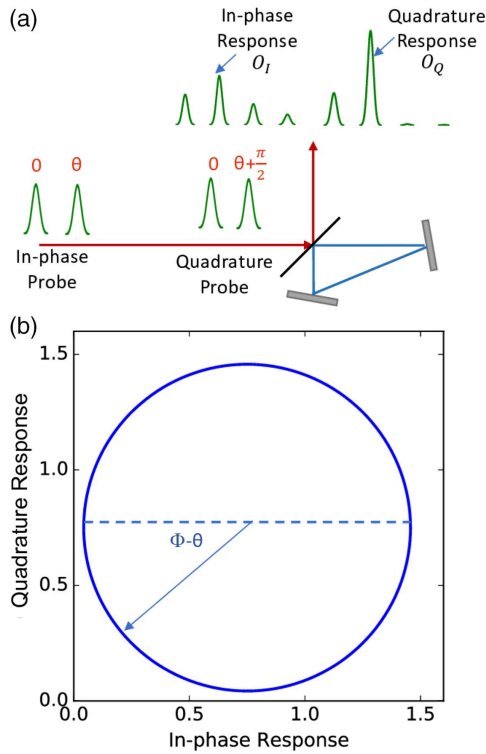


Fig. 6. In-phase response versus quadrature response at a single cavity, and resultant phase plot.

which is a sine function of the cavity phase. As shown in Fig. 6(a), one can define the first two-pulse burst as the “in-phase” probe and the second two-pulse burst with $\frac{\pi}{2}$ phase modulation as the “quadrature” probe, while their respective second output pulses are the in-phase and quadrature response pulses. Thus, we have in-phase and quadrature intensity signals to reconstruct the optical phase angle.

Figure 6(b) relates the in-phase and quadrature response to the cavity phase, describing a circle as these values co-vary, with the angle with respect to the in-phase axis being $\phi - \theta$. Since the phase is derived from a variation of the impulse response using a modulated probe, the method can be called “modulated impulse response.”

C. MIR Detection for Multi-Stage Cascaded Coherent Pulse Stacking

One can extend the MIR concept to measure cavity phases in multi-cavity systems. The first cavity in a stage can be measured as described in the previous section. The second cavity can be measured using the first two output pulses from the in-phase and quadrature responses of the first cavity, as is shown in Fig. 7. In this case, the pulses incident on the second cavity will not have equal amplitude or the same set of relative phases as the first probe pulse bursts. In general, we can write the two incident probe pulses as

$$\mathbf{i}_n = \delta[n + 1] + k\delta[n]e^{j\theta}. \quad (12)$$

The intensity of the second response pulse from the cavity will be

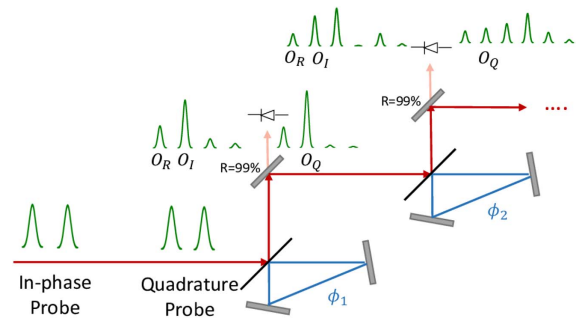


Fig. 7. In-phase and quadrature responses at cascaded, multi-cavity stackers.

$$O_0 = (1 - r^2)^2 + k^2 r^2 - 2kr(1 - r^2) \cos(\phi - \theta), \quad (13)$$

where k and θ are functions of previous cavity phases. Assuming that these previous cavities are constant because the previous cavities are well-controlled sequentially, one can write the intensity of the second response pulses O_I and O_Q as

$$O_I = A + B \cos(\phi - \theta_1), \quad (14a)$$

$$O_Q = C + D \cos(\phi - \theta_2), \quad (14b)$$

where θ_1 and θ_2 remain constant, and B and D are the range values $\frac{Max-Min}{2}$ of O_I and O_Q as ϕ varies. One then derives the cavity phase from

$$2 \cos\left(\frac{\theta_1 - \theta_2}{2}\right) \cos\left(\phi - \frac{\theta_1 + \theta_2}{2}\right) = \frac{DO_I + BO_Q - K_1}{BD}, \quad (15a)$$

$$-2 \sin\left(\frac{\theta_1 - \theta_2}{2}\right) \sin\left(\phi - \frac{\theta_1 + \theta_2}{2}\right) = \frac{DO_I - BO_Q - K_2}{BD}, \quad (15b)$$

where $K_1 = AD + BC$ and $K_2 = AD - BC$. Thus, we still can get the $\cos(\phi - \theta)$ and $\sin(\phi - \theta)$ values for the subsequent cavities, extending the phase detection to all cavities in a stage, by measuring the second response pulse in two cases.

In a multi-stage cascaded stacking scheme, there are different cavity lengths associated with each stage. For example, in the 2 + 2 stacking scheme of Fig. 3, there are two one-pulse-period-long cavities in stage one, and two five-pulse-period-long cavities in stage two. For each stage, the MIR method requires that the time interval between the pulses in the probe pulse burst is equal to the cavity round-trip time. Thus, there are two kinds of phase probe bursts, with either one pulse period or five periods between pulses, and these probes are sent at different times.

The accuracy of the MIR phase measurement depends on the accuracies of determining O_I and O_Q . The cavity phase error depends on the error in measuring these intensities to

$$\delta\phi = \sqrt{\left(p_I \frac{\delta O_I}{B}\right)^2 + \left(p_Q \frac{\delta O_Q}{D}\right)^2}, \quad (16)$$

where p_I and p_Q are phase-dependent parameters. We have $p_I = p_Q = 1$ when θ_1 and θ_2 have a $\frac{\pi}{2}$ phase difference. Better signal-to-noise ratios in the intensity measurements lead to better phase measurement accuracies. In addition, a higher k value in Eq. (12) will also improve the phase accuracy by increasing the intensity range values B and D in Eq. (16). Higher k values for subsequent cavities can be optimized by tuning the θ values in Eqs. (6) and (9), allowing optimized accuracy for the stage overall, preventing unfortunate values of θ from harming the measurement accuracy for certain cavities.

D. MIR Implementation on a FPGA

The MIR phase detection method has been successfully implemented on a field-programmable gate array (FPGA) [16]. These devices can process signals with much lower latency than a computer and can therefore implement complex control algorithms with more bandwidth and better noise suppression. Since the pulse duration in the experiment is shorter than the photodiode detector impulse response, we measure pulse energy, integrating in both space and time. Calculations of intensity are thus validated by measurements of energy with photodiode detectors, since beam size and pulse duration on the photodiode are constant during the experiment.

The measurement procedure involves three steps. First, pulse energy values are acquired at a high repetition rate and averaged to reduce wideband electronic amplifier noise. Three pulses are measured: the first reflected pulse is O_{-1} , used as a reference, and the other two pulses are O_I and O_Q . The second step is to calculate the I component $\cos \phi$ and Q component $\sin \phi$ based on Eq. (15). In the third step, the cavity phase is retrieved using these values. Using an FPGA, the phase can be determined within one microsecond, enabling high-speed control.

In principle, the coefficients A , B , C , and D in Eq. (15) can be directly derived based on Eq. (11), but experimental calibration of the pulse energy measurements can help improve accuracy by correcting constant errors. Figure 8 shows an example of calibration results. In this procedure, input and output energies are monitored, while the cavity phase is swept by continuously varying the voltage on the piezoelectric positioner. The A , B , C , and D values can be then corrected based on these curves.

Figure 9 shows the measured phase of one cavity as the phase is continuously varied by sweeping the piezo voltage. Detection resolution is about 4 mrad, determined mainly by

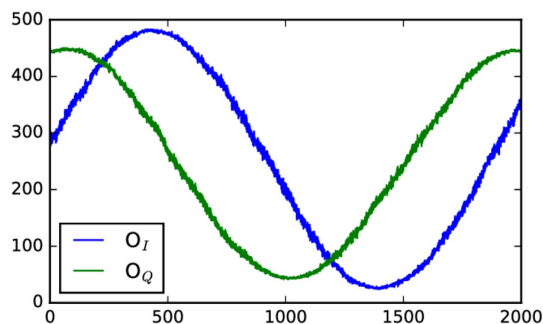


Fig. 8. Actual experimental calibration data of O_I and O_Q based on Eq. (15).

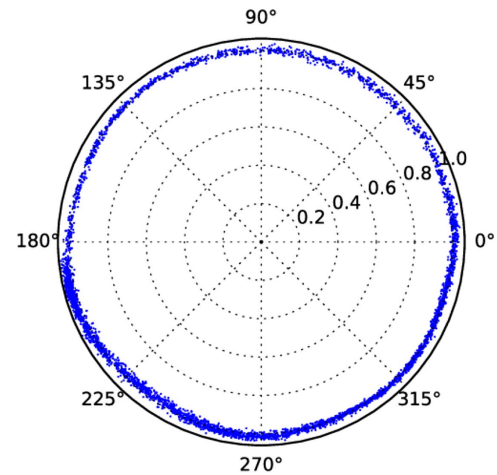


Fig. 9. Phase readout data while sweeping the cavity phase using the piezo controller.

the source laser amplitude noise and electronic noise in amplified photodiodes.

An example of the usefulness of high-speed phase detection is shown in Fig. 10, where a piezo-actuated cavity mirror is “pinged” with a step function, and the step response is determined by measuring the cavity phase directly. With this data, we can derive the complex response function of the mirror and design the control loop to optimize gain. Currently, the actuated mirror bandwidth is about 1.8 kHz, based on these measurements.

4. EXPERIMENTAL DEMONSTRATION

A. Experimental Setup

We demonstrated our MIR control scheme using a two-stage, $2 + 2$ (25 pulse) arrangement of cavities, part of a planned $2 + 2 + 2$ (125 pulse) stacker we are developing. The optical system is shown in Fig. 11. A semiconductor saturable absorber mirror (SESAM)-mode-locked Nd:Yag laser was the pulse source, producing 1064 nm, 10 ps pulses at 400 MHz. The output was coupled into fiber and modulated in amplitude and phase using LiNbO_3 waveguide modulators. The modulated

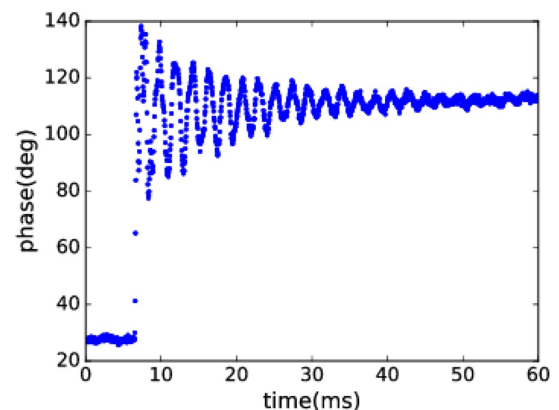


Fig. 10. Time-resolved step response measurement of a cavity with step applied to the piezo controlled mirror.

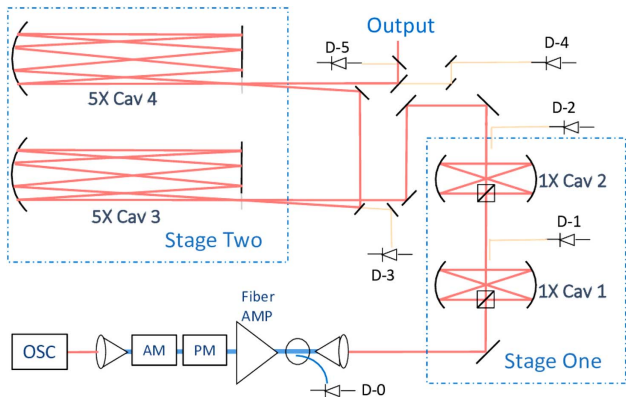


Fig. 11. 2 + 2 stacking experiment setup, showing the pulse burst source and two stacking stages.

light emerged into free space and was directed into Herriott cell cavities consisting of concave mirrors, which exhibit phenomenal stability due to their ability to relay a complex input amplitude to the output [22]. For certain values of mirror radii and spacing, an input laser beam was reproduced at the output, with the same position, angle, beam size, and divergence, enabling efficient interference at the interferometer input mirror. Furthermore, this relay function is insensitive to misalignment of the mirrors, as long as the beam remains in the cavity.

The two lengths of cavity were designed differently. In the short, one-pulse-period (1x) cavity, a 50% beam splitter cube, acting as the input/output low-reflectivity mirror, was placed between concave mirrors spaced by their radius, resulting in two bounces on each mirror. For the longer, five-pulse-period (5x) cavity, a similar optical design was effectively folded at a flat mirror at the center of the cavity, so that the actual cavity consisted of one curved mirror and one flat, with a quarter of the flat mirror coated for 50% reflectivity (the input/output surface), and the rest of it high-reflecting. There were four reflections of the beam per mirror, with the round-trip being 8 times the mirror spacing, resulting in a compact arrangement. There is one photodiode for each cavity, detecting the optical phase via the MIR method.

B. Time-Multiplexed Control With FPGA

An FPGA-based data-acquisition system was developed for the stacking experiment, with two high-speed (1 GHz) analog to digital converters (ADCs) and two digital to analog converters (DACs) [16] with the data flow as shown in Fig. 12. The fast DACs controlled the amplitude and phase of each pulse in the train, while the resultant pulse energies sensed by photodiodes were read by the two fast ADCs. We multiplexed six pulse signals onto the two ADCs using analog switches controlled by a set of slow DACs, which also controlled the piezo actuators in the cavities. The FPGA was clocked at the mode-locked oscillator repetition rate.

Probe pulse bursts to address the short and long cavities were generated by the high-speed, electro-optic amplitude and phase modulators. In a practical amplifier system, the output pulse repetition rate is limited by the energy storage time in the amplifier medium, if maximum energy is required, which

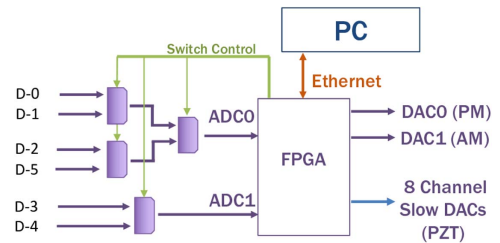


Fig. 12. Data flow in the CPS controller.

leads to 1–10 kHz repetition rates for Yb-doped fiber. Cavity phase detection could be done at higher rates to fully suppress acoustic noise, avoiding bandwidth limits otherwise imposed by the main pulse repetition rate. In addition, test pulses were used to sense the amplitude modulator bias point to maintain maximum extinction. Thus, we multiplexed probe and stacking pulse trains, in addition to other test pulses, as shown in Fig. 13.

Multiple pulse bursts occupied different time segments, occurring at different repetition rates. Some of the interleaving was to allow time to switch different sensors into the two fast ADCs. The stacking burst operated at 6.6 kHz, the stage-one I and Q probe bursts operated at 20 kHz, and the stage-two probe bursts operated at 80 kHz. With a typically 5 μs interval between bursts, all optical energy from the previous burst was gone before the next burst appeared.

C. Cavity Optical Phase Locking

All the cavity round-trip phases in our experiment were measured, and control loops were implemented to maintain stable optimization of each cavity. The control loops were operating at 1.2 KHz. Figure 14(a) compares the noise spectrum of a 1x short cavity when the control loop was open and when it was closed (i.e., locked to a specified value). Figure 14(b) shows the same comparison for a 5x cavity. Below 1 Hz, thermal drift was dominant, while above 1 Hz, air turbulence and acoustic noise were the main perturbations. Above 500 Hz, oscillator amplitude noise and electronic amplifier noise were the primary sources. Acoustic and thermal perturbations were larger for the longer cavity.

The air turbulence was significantly reduced by enclosing the optical cavities into either boxes or tubes, and the acoustic noise was reduced somewhat by floating the optical table. Measurements of oscillator amplitude/phase noise and adjustments of the oscillator cavity indicated that some large noise features, such as the peak at 140 Hz, were due to this source. This interpretation was supported by the fact that this peak contributed 5 times as much to the 5x cavity noise (25 mrad)

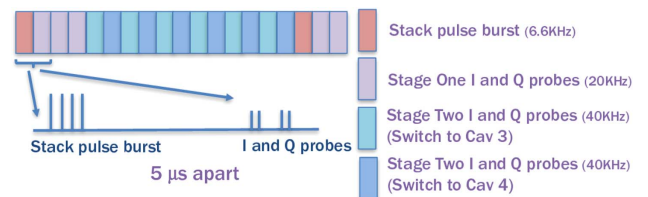


Fig. 13. Time multiplexing of multiple pulse bursts, occurring at different repetition rates.

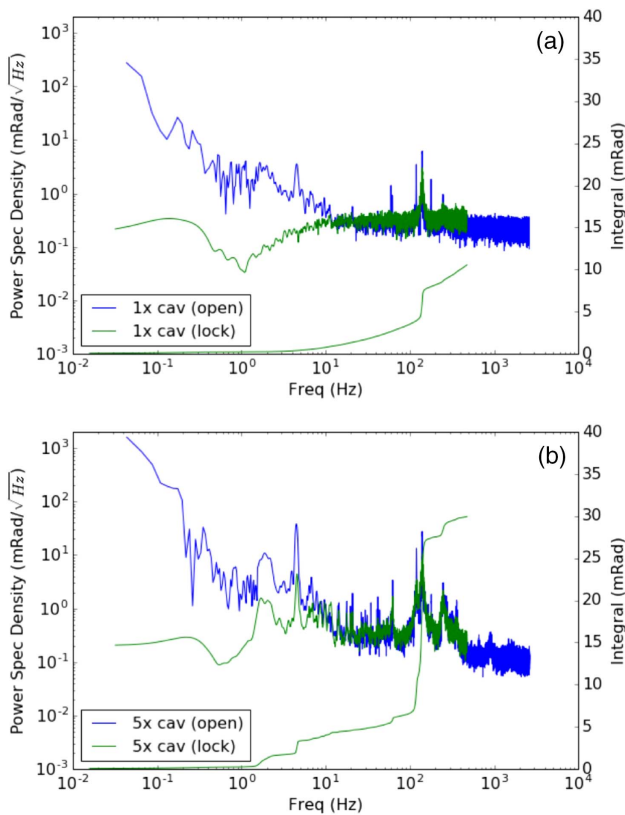


Fig. 14. Phase noise spectrum comparison of (a) 1× cavity and (b) 5× cavity between open-loop and closed-loop cases.

as it did to the 1× cavity noise (5 mrad), and we observed that the 140 Hz noise peak magnitude changed when we tuned the oscillator cavity mirror.

The control loops were operating at 1.3 kHz, which indicated that the unity gain bandwidth should be around 130 Hz. However, the oscillator intensity noise and photodiode amplifier electronic noise led to a high noise floor, which intersected the approximately $1/f$ phase noise at low frequencies. Probe pulses were produced and analyzed at a repetition rate of as high as 80 kHz, allowing high-frequency noise to be averaged down with digital filters in the FPGA firmware. While the noise floor was reduced, it was still large enough to intersect the phase noise at around 10 Hz. Even with this bandwidth limitation, we were able to control the 1× cavity to within 15 mrad and the 5× cavity to within 35 mrad. If these were the only sources of noise on the stacked pulse energy, this would be enough to guarantee far less than 1% stability, according to Fig. 5(b).

D. Stacking Result and Stability

The MIR phase control method was used to demonstrate stacking of 25 pulses in the 2 + 2 arrangement. The initial target values for cavity phase were based on numerical simulation, but an optimization loop was also operating at 0.05 Hz to adjust these set-point values to maximize output pulse amplitude. A 16-bit sampling scope (Keysight 86100D) was used to monitor the stacked output pulses and input pulses, as shown in Fig. 15. In that figure, ringing in the photodiode contributes to post-pulse amplitude after the main pulse.

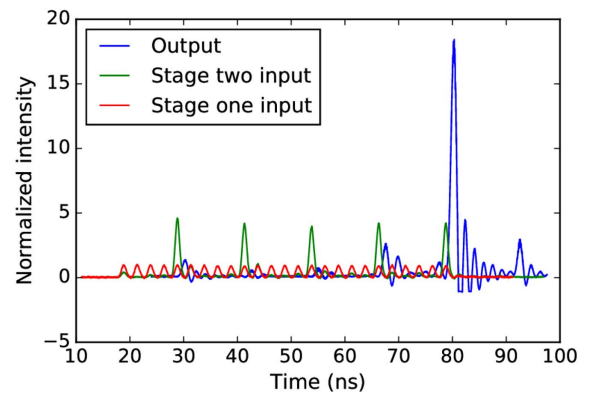


Fig. 15. The 25-pulse stacking experimental result. The output (blue curve), stage-two input (green curve), and stage-one input (red curve) are compared.

Energy enhancement of 18.4 was achieved, compared with a theoretical value of 21.5. Stage one operated best, generating five pulses cleanly, but the second stage exhibited large pre- and post-pulse amplitudes, decreasing the stacking efficiency. We had observed during alignment that the intra-cavity pulses in the long cavities were not superimposed, preventing efficient interference, and subsequent measurements confirmed that the mirror radii were off by about 3% from their optimum value. This, we believe, is the main limitation to efficiency in the second stage.

The short-term output stability was measured to be 1.1% over 1 Hz to 3.3 kHz, as shown in Fig. 16, reading the blue curve and its integral. As mentioned previously, the cavity phase noise performance implied that the stacked pulse stability should be better than this, as indicated by the green curve and its integral, where the phase noise data was used to numerically predict the stacked pulse amplitude. When we superimposed the laser power noise spectrum, it appears that most of the observed stacked pulse energy noise was due to that. The main contribution of the phase noise was at 140 Hz, where oscillator phase noise dominated both measurement and final

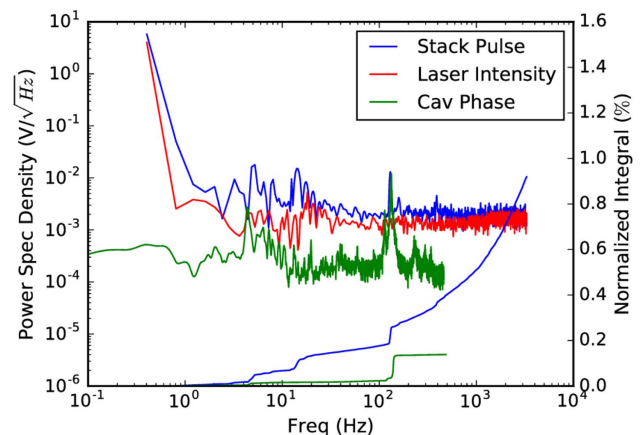


Fig. 16. Stacked pulse energy noise spectrum (blue curve) is compared with the laser pulse energy stability (red curve) and the spectrum derived from cavity phase errors (green curve). The integrals based on the blue curve and green curve are also shown.

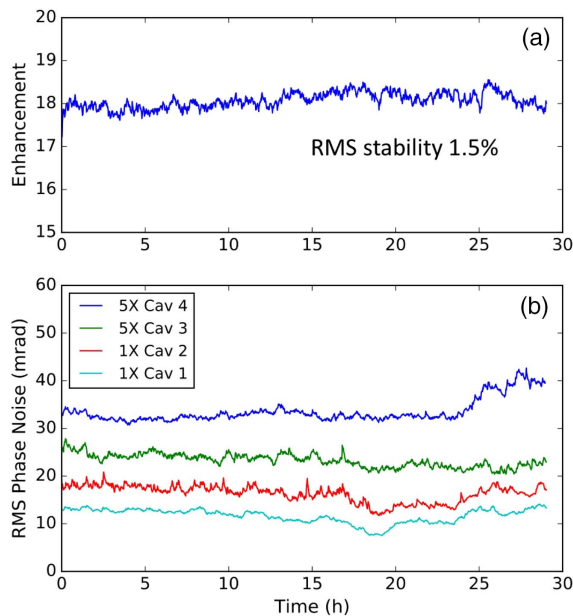


Fig. 17. Long-term stability measurements. (a) Final pulse enhancement value. (b) RMS phase noise of all optical cavities.

output processes. We can say that the cavity phase noise has been reduced to a point where it is not the main issue.

Long-term stability is shown in Fig. 17, where the output stability was maintained to 1.5% for 30 h, and the phase noises of the four cavities were kept well below 50 mrad during this time. The RMS phase noise of the second cavities in each stage was stronger than the noise of the first cavities. This was because within each stage, the second-cavity phase probe pulse measurement was slightly modified by the noise in the previous cavity, making the second-cavity RMS phase noise larger than the first. In addition, the 5× cavities were noisier than the 1× cavities because 5× cavities were more easily affected by environmental perturbations and they were more sensitive to oscillator phase noise. As interferometers, the longer cavities are a more stringent measurement of the oscillator coherence length.

5. CONCLUSIONS

We have described a novel method of interrogating optical cavities used for temporal pulse addition, using a sophisticated variation of impulse response measurement. Because measurements are made of each cavity in parallel, the data acquisition time does not increase with the number of cavities, enabling high bandwidth control of complex temporal stacking systems as well as individual characterization of the noise from each cavity. The method can be implemented in an FPGA, providing high-speed detection and correction, resulting in megahertz (MHz) measurement rates. This method can be extended to any number of cavities by increasing the number of channels of data processing hardware.

A demonstration of the MIR cavity phase measurement method has shown that it can be used to measure and control four stacking cavities and can provide much less than 1–1.5% short- and long-term stability of the resultant stacked pulse.

This method is an effective way to control temporal combination in high-intensity ultrafast fiber.

Funding. U.S. Department of Energy (DOE) (DE-AC02-05CH11231).

REFERENCES

1. M. N. Zervas and C. A. Codemard, "High power fiber lasers: a review," *IEEE J. Sel. Top. Quantum Electron.* **20**, 219–241 (2014).
2. J. Limpert, A. Klenke, M. Kienel, S. Breikopf, T. Eidam, S. Hädrich, C. Jauregui, and A. Tünnermann, "Performance scaling of ultrafast laser systems by coherent addition of femtosecond pulses," *IEEE J. Sel. Top. Quantum Electron.* **20**, 268–277 (2014).
3. G. Mourou, B. Brocklesby, T. Tajima, and J. Limpert, "The future is fibre accelerators," *Nat. Photonics* **7**, 258–261 (2013).
4. E. Esarey, C. B. Schroeder, and W. P. Leemans, "Physics of laser-driven plasma-based electron accelerators," *Rev. Mod. Phys.* **81**, 1229–1285 (2009).
5. A. Galvanauskas, A. Hariharan, D. Harter, M. A. Arbore, and M. M. Fejer, "High-energy femtosecond pulse amplification in a quasi-phase-matched parametric amplifier," *Opt. Lett.* **23**, 210–212 (1998).
6. T. Eidam, J. Rothhardt, F. Stutzki, F. Jansen, S. Hädrich, H. Carstens, C. Jauregui, J. Limpert, and A. Tünnermann, "Fiber chirped-pulse amplification system emitting 3.8 GW peak power," *Opt. Express* **19**, 255–260 (2011).
7. J. Ruppe, "Theoretical and experimental foundations of coherent pulse stacking amplification," Ph.D. thesis (University of Michigan, 2017).
8. S. Zhou, F. W. Wise, and D. G. Ouzounov, "Divided-pulse amplification of ultrashort pulses," *Opt. Lett.* **32**, 871–873 (2007).
9. Y. Zaouter, F. Guichard, L. Daniault, M. Hanna, F. Morin, C. Hönninger, E. Mottay, F. Druon, and P. Georges, "Femtosecond fiber chirped- and divided-pulse amplification system," *Opt. Lett.* **38**, 106–108 (2013).
10. S. Breikopf, T. Eidam, A. Klenke, L. Von Grafenstein, H. Carstens, S. Holzberger, E. Fill, T. Schreiber, F. Krausz, A. Tünnermann, I. Pupeza, and J. Limpert, "A concept for multiterawatt fibre lasers based on coherent pulse stacking in passive cavities," *Light: Sci. Appl.* **3**, e211 (2014).
11. T. Zhou, J. Ruppe, C. Zhu, I.-N. Hu, J. Nees, and A. Galvanauskas, "Coherent pulse stacking amplification using low-finesse Gires-Tournois interferometers," *Opt. Express* **23**, 7442–7462 (2015).
12. T. Zhou, J. Ruppe, P. Stanfield, J. Nees, R. Wilcox, and A. Galvanauskas, "Resonant cavity based time-domain multiplexing techniques for coherently combined fiber laser systems," *Eur. Phys. J. Spec. Top.* **224**, 2585–2602 (2015).
13. J. Ruppe, S. Chen, M. Sheikhsofla, R. Wilcox, J. Nees, and A. Galvanauskas, "Multiplexed coherent pulse stacking of 27 pulses in a 4 + 1 gti resonator sequence," in *Proceedings of ASSL Conference* (Optical Society of America, 2016), paper AM4A.6.
14. Y. Yang, J. Byrd, J. Dawson, L. Doolittle, A. Galvanauskas, G. Huang, W. Leemans, D. Qiang, J. Ruppe, and R. Wilcox, "Multicavity coherent pulse stacking using Herriott cells," in *North American Particle Accelerator Conference (NAPAC) (JACOW, 2017)*, pp. 370–372.
15. H. Pei, J. Ruppe, S. Chen, M. Sheikhsofla, J. Nees, Y. Yang, R. Wilcox, W. Leemans, and A. Galvanauskas, "10 mj energy extraction from Yb-doped 85 μm core CCC fiber using coherent pulse stacking amplification of fs pulses," in *Proceedings of ASSL Conference* (Optical Society of America, 2017), paper AW4 A.4.
16. Y. Xu, R. Wilcox, J. Byrd, L. Doolittle, Q. Du, G. Huang, Y. Yang, T. Zhou, W. Leemans, A. Galvanauskas, J. Ruppe, C. Tang, and W. Huang, "FPGA-based optical cavity phase stabilization for coherent pulse stacking," *IEEE J. Quantum Electron.* **54**, 1–11 (2018).
17. M. Kienel, A. Klenke, T. Eidam, M. Baumgartl, C. Jauregui, J. Limpert, and A. Tünnermann, "Analysis of passively combined divided-pulse amplification as an energy-scaling concept," *Opt. Express* **21**, 29031–29042 (2013).
18. M. Kienel, A. Klenke, T. Eidam, S. Hädrich, J. Limpert, and A. Tünnermann, "Energy scaling of femtosecond amplifiers using

- actively controlled divided-pulse amplification," *Opt. Lett.* **39**, 1049–1052 (2014).
19. R. W. P. Drever, J. L. Hall, F. V. Kowalski, J. Hough, G. M. Ford, A. J. Munley, and H. Ward, "Laser phase and frequency stabilization using an optical resonator," *Appl. Phys. B* **31**, 97–105 (1983).
 20. M. A. Vorontsov, G. W. Carhart, and J. C. Ricklin, "Adaptive phase-distortion correction based on parallel gradient-descent optimization," *Opt. Lett.* **22**, 907–909 (1997).
 21. H. Pei, J. Ruppe, S. Chen, M. Sheikhsofla, J. Nees, Y. Yang, W. L. Russell Wilcox, and A. Galvanauskas, "Near-complete stored energy extraction from fiber amplifiers in ultrashort > 10 mJ energy pulses using coherent pulse stacking amplification," *Proc. SPIE* **10512**, 1051209 (2018).
 22. D. Dahlen, R. Wilcox, and W. Leemans, "Modeling Herriott cells using the linear canonical transform," *Appl. Opt.* **56**, 267–272 (2017).